Explainable Eigenvalue-Based Identification of Inverter Dynamics

Hanshan Qing[1], *Student Member, IEEE,* Abhinav Kumar Singh[1], *Member, IEEE,* Efstratios Batzelis[1], *Senior Member, IEEE,*

[1] *School of Electronics and Computer Science, University of Southampton, Southampton, United Kingdom*
H.Qing@soton.ac.uk, A.K.Singh@soton.ac.uk, E.Batzelis@soton.ac.uk

***Abstract*—The proliferation of inverter-based resources (IBRs) presents a significant modeling challenge, creating a dichotomy between intractable first-principles (white-box) models and uninterpretable, purely data-driven (black-box) models. This paper introduces a framework that bridges this chasm by identifying an explainable, grey-box model for inverters from passive operational data. The methodology employs a Koopman autoencoder to discern the system's underlying linear dynamics in a latent space, from which dominant system eigenvalues are subsequently extracted. This process yields a physically meaningful, control-oriented linear model without requiring knowledge of the inverter's proprietary internal structure. The efficacy of the proposed framework is rigorously validated by comparing its captured eigenvalues and open-loop transient response against a high-fidelity benchmark, demonstrating high accuracy in capturing the true system dynamics.**

***Index Terms*—System Identification, Explainable AI, Grey-Box Modeling, Power Inverters, Data-Driven Modeling, Eigenvalue Analysis, Passive System Identification.**

I. Introduction

The increasing integration of inverter-based resources (IBRs) fundamentally alters power grid dynamics [1], making accurate dynamic models essential for stability analysis and control design. Developing such models, however, faces two key challenges: first, traditional white-box models are often unavailable due to proprietary controls [2], and second, obtaining informative data is difficult. Many identification methods rely on *active perturbations*, such as frequency sweeping, which inject disturbances into the system. While effective, these approaches are intrusive and potentially destabilizing, rendering them unsuitable for online monitoring. Consequently, practitioners must rely on purely data-driven black-box models, which often lack interpretability [3], or on models identified from *passive* operational data, which is a significantly more challenging task.

System identification aims to construct mathematical models from data [4], spanning physics-based white-box models to data-driven black-box models [5], with grey-box approaches incorporating partial physical knowledge [6]. Classical techniques exist for Linear Time-Invariant (LTI) [7] and nonlinear systems [8]. Traditional linear methods, such as AutoRegressive Moving Average with eXogenous inputs (ARMAX), assume a fixed linear structure around an operating point [9]. While effective in strictly linear regimes, they struggle with nonlinearities such as control saturation and mode switching that are common in modern IBRs. Koopman operator theory offers an alternative by lifting nonlinear dynamics into a linear representation in a high-dimensional latent space, enabling linear analysis and control [10]. This has facilitated the use of Koopman-based models with control strategies such as model predictive control (MPC) [11] and linear–quadratic regulator (LQR) [12], often via deep autoencoders [13].

Despite the promise of Koopman-based methods, a key gap remains: existing work often assumes access to a high-fidelity model, while the reliable identification of an *explainable*, eigenvalue-based latent model from *passive, non-intrusive operational data* has received limited attention. To address this gap, we employ a Koopman autoencoder [14] that requires no detailed parameter knowledge, incorporates physical constraints, and yields an interpretable linear latent model from which dominant system eigenvalues can be directly extracted. This approach is particularly valuable for practical applications where theoretical models may not match field reality. Specifically, it facilitates real-time stability assessment using actual measured data, and allows for the modeling of IP-protected systems where internal control structures are proprietary and unknown. The main contributions are:

- **A Grey-Box Identification Framework:** A practical framework that bridges white-box and black-box paradigms by identifying physically meaningful models without access to proprietary internal details.
- **Explainable Eigenvalue-Based Modeling:** Direct extraction of dominant system eigenvalues, providing interpretable insight into stability and dynamic behavior suitable for control design.
- **Identification from Passive Data:** A methodology explicitly designed for passive operational data, enhancing practical applicability. Although validated using simulation data with known ground truth, the framework is intended for direct training on measured time-series data from field devices (e.g., phasor measurement units).

II. Methodology

The proposed identification framework, illustrated in Fig. 1, follows a two-stage process: an iterative training stage to generate an ensemble of candidate models, followed by a robust post-processing stage to extract the final, stable system

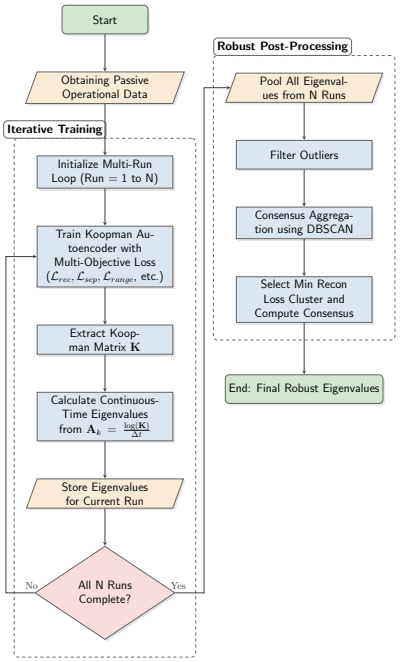

Fig. 1: Flowchart of the proposed data-driven identification algorithm, detailing the iterative training and robust post-processing stages.

eigenvalues. The following subsections detail the mathematical underpinnings of each step in this workflow.

A. System Representation and Problem Formulation

The dynamic behavior of an inverter around a steady-state operating point can be represented by a state-space model:

$$\dot{\mathbf{x}}(t) = \mathbf{A}\mathbf{x}(t) + \mathbf{B}\mathbf{u}(t), \qquad \mathbf{z}(t) = \mathbf{C}\mathbf{x}(t) + \mathbf{D}\mathbf{u}(t) \tag{1}$$

where $\mathbf{x}(t)$ are the true (but unknown) system states, $\mathbf{u}(t)$ is the control input vector, and $\mathbf{z}(t)$ is the measurement vector. The system matrix $\mathbf{A}$ contains the eigenvalues that govern the system's dynamic response. The objective of system identification is to determine the dynamics from the measured data $(\mathbf{u}(t), \mathbf{z}(t))$ that accurately represent the true system.

B. Koopman Autoencoder for Dynamic Modeling

At the core of the proposed framework lies a Koopman autoencoder, a neural network architecture designed to learn linear dynamics from nonlinear measurement data [14]. The model consists of:

1) An Encoder (ϕ): An multi-layer perceptron (MLP) that maps the measurement vector $\mathbf{z}_k$ (containing current and possibly past measurements) to a latent-space representation $\hat{\mathbf{x}}_k \in \mathbb{R}^n$, which represents an estimate of the system's true states.
2) A Linear Dynamics Layer: A pair of matrices, $\mathbf{K}$ and $\mathbf{B}_d$, that propagate the latent state $\hat{\mathbf{x}}_k$ forward in discrete time according to the Koopman operator principle:

$$\hat{\mathbf{x}}_{k+1} = \mathbf{K}\hat{\mathbf{x}}_k + \mathbf{B}_d\mathbf{u}_k \tag{2}$$

3) A Decoder (ψ): A second MLP that maps the latent state $\hat{\mathbf{x}}_k$ back to the measurement space, reconstructing the system's measurements $\hat{\mathbf{z}}_k$.

To ensure physical consistency, the eigenvalues λ_i of the learned Koopman matrix $\mathbf{K}$ are parameterized. They are explicitly defined as either real eigenvalues, representing non-oscillatory modes, or as complex conjugate pairs, representing oscillatory modes. A complex conjugate pair is parameterized by its natural frequency ω_n and damping ratio ζ as $\lambda = e^{(-\zeta\omega_n \pm j\omega_n\sqrt{1-\zeta^2})\Delta t}$.

This parameterization allows the model to be trained by directly optimizing for physically meaningful quantities (ω_n, ζ) rather than abstract matrix entries.

C. Data-Driven Constraints

To ensure the identified model is physically plausible and adheres to engineering characteristics, a set of data-driven constraints is imposed during training to improve convergence.

1) Frequency Range Constraints: Based on typical inverter control structures, the oscillatory modes are constrained to expected frequency bands (e.g., Low-Pass Filter mode: 3-5.5 Hz, Controller mode: 10-70 Hz) [15]–[18].
2) Damping Ratio Constraints: Based on control theory principles, all damping ratios ζ are constrained to a physically realistic range (e.g., $0.1 < \zeta < 0.8$) to represent underdamped but stable systems [19]. A minimum separation between modes is also enforced.
3) Stability Constraints: All identified eigenvalues are constrained to have negative real parts, enforcing that the identified system is stable. This constraint is grounded in the physical reality that the training data is collected from stable operations; thus, the model must reflect stable dynamics. Unstable modes would manifest as diverging trajectories not present in standard operational data.

D. Training Methodology

The model is trained using a multi-phase approach to balance the competing objectives of accurate reconstruction and physical plausibility.

1) Main Training: The model is first trained with a balanced optimization of all objectives.
2) Frequency Focus: Training emphasis is shifted to prioritize accurate learning of modal frequencies.
3) Damping Focus: Training emphasis is shifted to refine the damping ratios of the identified modes.

This process is governed by a composite loss function $\mathcal{L}$ that combines a primary reconstruction objective with penalties for constraint violations:

$$\begin{aligned}\mathcal{L} = w_{rec}\mathcal{L}_{rec} + w_{stab}\mathcal{L}_{stab} + w_{range}\mathcal{L}_{range} + \\ w_{sep}\mathcal{L}_{sep} + w_{damp}\mathcal{L}_{damp} + w_{div}\mathcal{L}_{div}\end{aligned} \tag{3}$$

where:

- $\mathcal{L}_{rec}$: Reconstruction loss measures the difference between true measurements $\mathbf{z}_k$ and reconstructed measurements $\hat{\mathbf{z}}_k = \psi(\hat{\mathbf{x}}_k)$ over a time series of length T, calculated as $\mathcal{L}_{rec} = \frac{1}{T}\sum_{k=1}^{T} ||\mathbf{z}_k - \hat{\mathbf{z}}_k||^2$.
- $\mathcal{L}_{stab}$: Stability penalty sums the positive real parts of all eigenvalues, using the rectified linear unit (ReLU) function $\max(0, x)$, computed as $\mathcal{L}_{stab} = \sum_{i=1}^{n} \text{ReLU}(\text{Re}(\lambda_i))$.
- $\mathcal{L}_{\omega\_range}$: Frequency range penalty sums violations outside predefined bounds $[\omega_{\min,i}, \omega_{\max,i}]$ for each oscillatory mode, given by $\mathcal{L}_{\omega\_range} = \sum_{i\in\text{Osc}} (\text{ReLU}(\omega_i - \omega_{\max,i}) + \text{ReLU}(\omega_{\min,i} - \omega_i))$.
- $\mathcal{L}_{\zeta\_range}$: Damping range penalty sums violations outside predefined bounds $[\zeta_{\min}, \zeta_{\max}]$, calculated as $\mathcal{L}_{\zeta\_range} = \sum_{i\in\text{Osc}} (\text{ReLU}(\zeta_i - \zeta_{\max}) + \text{ReLU}(\zeta_{\min} - \zeta_i))$.
- $\mathcal{L}_{sep}$: Separation penalty enforces minimum frequency difference $\Delta\omega_{\min}$ between adjacent oscillatory modes (assuming frequencies ω_i are sorted), computed as $\mathcal{L}_{sep} = \sum_{i=1}^{m-1} \text{ReLU}(\Delta\omega_{\min} - (\omega_{i+1} - \omega_i))$.
- $\mathcal{L}_{div}$: Diversity penalty encourages modes to be distinct, penalizing small differences between all pairs of frequencies and damping ratios using $\mathcal{L}_{div} = \sum_{i\neq j} \left(e^{-\alpha|\omega_i-\omega_j|} + e^{-\beta|\zeta_i-\zeta_j|}\right)$, where $\alpha, \beta > 0$ control the sensitivity.

E. Extraction of Continuous-Time State-Space Model

After training, the learned discrete-time Koopman matrix $\mathbf{K}$ is used to derive the continuous-time system matrix $\mathbf{A}_k$ via the matrix logarithm $\mathbf{A}_k = \frac{\log(\mathbf{K})}{\Delta t}$, where Δt is the sampling time of the data. The eigenvalues of this resulting matrix $\mathbf{A}_k$ represent the identified continuous-time modes of the inverter system.

F. Robust Eigenvalue Estimation via Consensus Aggregation

Due to the stochastic nature of neural network training, which can lead to convergence in local minima, a multi-run ensemble approach is employed to ensure a robust and reliable estimate of the system's true modes. This "Consensus Aggregation" method replaces traditional single-run.

1) Train Ensemble: An ensemble of models (e.g., 50) is trained from different random initializations.
2) Collect Eigenvalues: The continuous-time eigenvalues are extracted from all models in the ensemble and pooled into a single set.
3) Filter Outliers: Latent dimensions or spurious modes (e.g., $|\text{Re}(\lambda)| > 1000$) are filtered out.
4) Cluster Eigenvalues: A density-based clustering algorithm (DBSCAN) is applied to the pooled eigenvalues in the 2D complex plane [20]. This groups similar eigenvalues identified across different training runs.
5) Compute Consensus: Cluster with the minimum reconstruction loss is taken for each mode. The final identified eigenvalue for each mode is taken as the median (real and imaginary parts) of all eigenvalues within its corresponding cluster. This median-based consensus is robust to outliers from any single failed training run.

This hybrid approach mitigates the impact of spurious results and provides a high-confidence estimate of the inverter's dominant dynamics without needing a ground-truth reference.

III. Case Study

A. Benchmark Model and Data Generation

The efficacy of the proposed methodology is validated against benchmark models, including a seventh-order grid-following (GFL) inverter and a fourth-order grid-forming (GFM) inverter. They are connected to a single machine infinite bus (SMIB), as shown in Fig. 2. The detailed model of GFL inverter can be found in [21]. The GFM model emulates the behavior of a synchronous machine and consists of four state variables: the machine angle (δ), the frequency (ω), and the d-q axis currents (i_d, i_q). The system dynamics are described by the swing equation and the electrical dynamics of the output filter, as shown in (4)-(7). The parameters used for this GFM model are: inertia constant $M = 10.0$, damping factor $D = 3.0$, droop gain $K_p = 5.0$, nominal power $P_{ref} = 1.0$ p.u., filter reactance $X_f = 0.1$ p.u., grid reactance $X_g = 0.05$ p.u., filter resistance $R_f = 0.01$ p.u., and grid resistance $R_g = 0.005$ p.u.

$$\dot{\delta} = \omega_r - \omega_s \tag{4}$$

$$\dot{\omega} = \frac{1}{M}(P_m - P_{e,mech} - D(\omega - 1.0)) \tag{5}$$

$$\dot{i}_d = \frac{1}{L_t}(E_d - R_t i_d - V_b + L_t \omega_r i_q) \tag{6}$$

$$\dot{i}_q = \frac{1}{L_t}(E_q - R_t i_q - L_t \omega_r i_d) \tag{7}$$

To generate a dynamically rich and informative dataset, the simulation model is subjected to a variety of passive excitations over a 2-second simulation period with a 1 kHz sampling rate, as shown in Fig. 2. These signals are designed to excite a wide range of dynamic modes by simulating plausible real-world operational conditions. The active power reference is subjected to multiple **step changes** (e.g., $1.0\,\text{p u}$ to $1.2\,\text{p u}$) and **ramp changes**, which emulate the fast response required for grid contingencies [22], [23] and gradual adjustments for economic dispatch [24], respectively. Simultaneously, the reactive power reference receives **step changes** (e.g., $0\,\text{p u}$ to $0.05\,\text{p u}$). To excite oscillatory modes, the grid voltage inputs (v_{gd}, v_{gq}) are injected with **multi-tone sinusoidal disturbances** at 3 Hz, 5 Hz and 7 Hz, simulating the natural, low-frequency power oscillations inherent in large, interconnected power systems [19], [25].

This process yields a comprehensive set of time-series trajectories for training the identification model, which is indicative and representative of passive data recorded in real systems. Only measurable data is used for training, which includes voltage and current in d and q axis and reference power. Then two networks, three layers for each encoder and decoder, with 7 and 4 latent states are trained separately for GFL and GFM inverters using the synthesized dataset. Frequency sweeping, conventional AE, ARMAX and proposed algorithm are validated on this dataset.

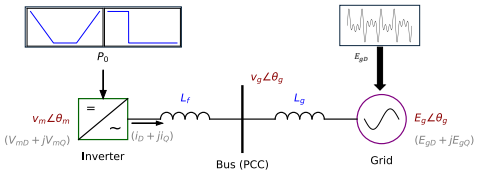

Fig. 2: Single-line diagram of the SMIB test system used for validation, showing the GFL inverter connected to the infinite grid through a filter and grid impedance.

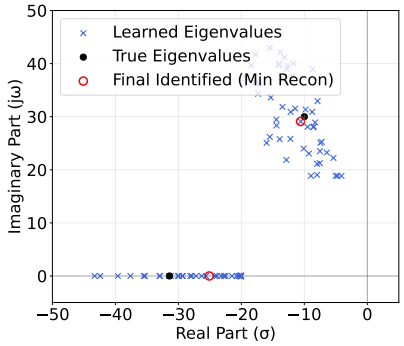

Fig. 3: S-plane plot for GFL case study. Identified cluster centers (red circles) show close agreement with the dominant true eigenvalues (black dot).

B. Results and Discussion

1) Grid-Following Inverter Analysis: A primary measure of the algorithm's performance is its ability to accurately identify the dominant eigenvalues of the true system. The detailed eigenvalue results for the GFL inverter, summarized in Table I, show a distinct performance advantage for the proposed algorithm. It successfully captures the dominant low-frequency oscillatory mode with high fidelity (2.9% frequency error, 8.2% damping error) as well as the key real pole.

Most critically, the proposed method always correctly identifies the system as stable. In sharp contrast, both benchmark black-box techniques (frequency sweeping and conventional AE) falsely predict instability, identifying multiple spurious modes with positive real parts (e.g., **+8.714**). Similarly, the ARMAX model, while linear, fails to capture the correct dynamics, yielding large errors. The benchmark model exhibits two high-frequency modes which correspond to the current controller and filter inductor current dynamics, respectively. These were outside the effective bandwidth of the identified model. As noted in the results, the absence of modes 3-6 in the identified model is attributed to the spectral characteristics of the passive training data. These modes likely lacked sufficient excitation to be distinguished from noise, as safe, practical excitation signals often lack the high-frequency transients required to excite them fully. The robustness of this identification is visually confirmed in Fig. 3.

2) Grid-Forming Inverter Analysis: To demonstrate versatility, the framework was applied to a GFM inverter. The results in Table I and Fig. 4 show it successfully identified

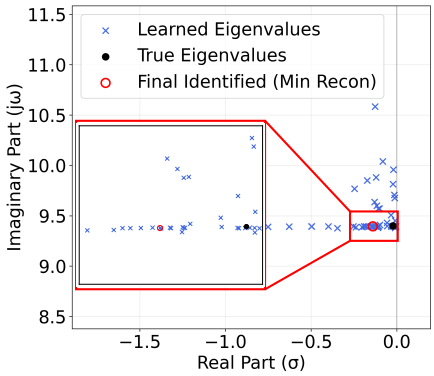

Fig. 4: S-plane plot for the GFM inverter case study, showing agreement between the true eigenvalues (black dot) and the identified cluster centers (red circles markers).

all system modes, including the low-frequency swing mode and the mid-frequency EM mode. While the swing mode was captured with moderate accuracy, the EM mode's damping was less precise (though the frequency was in the correct range), highlighting a trade-off. However, the benchmark methods failed entirely. The Frequency Sweeping method identified a spurious mode while missing the EM mode, and both benchmarks again predicted false instability.

3) Overall Performance and Model Reliability: The key finding, summarized in the 'Overall Performance Metrics' section of Table I, relates to model reliability. The proposed grey-box model was the *only* method to correctly predict stability for both inverter types. The black-box methods, while computationally faster, proved dangerously misleading. They consistently failed to distinguish true system dynamics from noise, resulting in false stability predictions (either unstable or spurious modes) in every case study. This underscores the value of the physically-constrained, grey-box approach for reliable stability assessment from passive data. The discrepancy in capturing similar frequency modes between GFL and GFM cases stems from the differing control architectures. In GFM inverters, the coupling between power loops and output voltage is stronger, rendering certain modes more observable in the passive voltage data compared to the GFL configuration, where this coupling is more indirect.

IV. Conclusion

This paper presented an explainable grey-box framework for data-driven identification of inverter dynamics that bridges white-box and black-box approaches. The key contribution is demonstrating that reliable, physically interpretable models can be identified from *passive* operational data. The resulting eigenvalue-based model supports online stability monitoring by providing direct insight into damping margins. Validation against high-fidelity benchmarks showed that the proposed method was the only approach to correctly capture the stability of both GFL and GFM inverters, whereas benchmark black-box methods produced inconsistent results, often predicting spurious or unstable modes. These findings highlight the

TABLE I: Comparison of Identified Eigenvalues and Performance Metrics for GFL and GFM Inverters.

Mode / Metric	True System	Frequency Sweeping (Passive Data)	Conventional AE	ARMAX	Proposed Algorithm
Grid-Following (GFL) Inverter - Eigenvalues					
Phase-Locked Loop	-10.0 + 30.0j	**+8.714** + 28.705j	-0.065 + 0.366j	-19.05 + 15.87j	-10.600 + 29.100j
Phase-Locked Loop	-10.0 - 30.0j	**+8.714** - 28.705j	-0.065 - 0.366j	-19.05 - 15.87j	-10.600 - 29.100j
Current Controller	-167.6 + 310.0j	**+0.228** + 59.935j	**+0.172**	-97.99	-74.400 + 278.100j
Current Controller	-167.6 - 310.0j	**+0.228** - 59.935j	-0.173	-195.03	-70.700 + 253.300j
Inductor Current (Filter)	-337.4 + 624.1j	**+1.844** + 13.546j	-0.114	-409.52 + 775.16j	-500.000
Inductor Current (Filter)	-337.4 - 624.1j	**+1.844** - 13.546j	**+0.053**	-409.52 - 775.16j	-600.000
Low-Pass Filter	-31.4	-178.303	-0.473	-31.45	-25.100
GFL Performance Metrics					
Avg. Damping Error (Dom. Mode)	–	**Unstable**	44.6%	142.93%	8.2%
Avg. Freq. Error (Dom. Mode)	–	7.2%	98.8%	47.09%	2.9%
Computation Time	–	2.38s	3.43mins	3.9s	5.16mins
GFM Inverter - Eigenvalues					
Swing	-0.136 + 14.217j	**+1.844** + 13.546j	-0.065 + 0.366j	-0.44	-0.128 + 9.396j
Swing	-0.136 - 14.217j	**+1.844** - 13.546j	-0.065 - 0.366j	-5.18	-0.128 - 9.396j
EM	-31.580 + 313.854j	-4.657 + 25.272j	**+0.172**	N/A	-4.022 + 335.476j
EM	-31.580 - 313.854j	-4.657 - 25.272j	-0.173	N/A	-4.022 - 335.476j
GFM Performance Metrics					
Damping Error (Dom. Mode)	–	**Unstable**	1650%	10,277.12%	42.4%
Freq. Error (Dom. Mode)	–	4.72%	97.4%	N/A%	33.9%
Computation Time	–	0.62s	2.37mins	0.8s	4.10mins
Overall Performance Metrics					
Model Type	–	Black-Box	Black-Box	Black-Box	Grey-Box
Stability Prediction	–	Incorrect	Incorrect	Incorrect	Correct

importance of embedding physical constraints in data-driven identification.

A current limitation is reduced accuracy for weakly excited or high-frequency modes. While this study used voltage and power reference signals, the framework is extensible. Future work will explore incorporating additional measurements, such as PCC frequency or internal current signals, which could improve observability of specific modes like the PLL, though this must be balanced against practical sensor availability.

ACKNOWLEDGMENT

This work has been conducted within UNIFORM project and supported by UKRI under Grant agreement EP/Y001575/1.

REFERENCES

[1] A. Ekic, "Impact of inverter-based resources on grid dynamics," Ph.D. dissertation, 2022.

[2] A. Dželo, A. Mešanović, and M. Cosovic, "Identification of black-box inverter-based resource control using hammerstein-wiener models," *arXiv preprint arXiv:2411.13213*, 2024.

[3] A. Ahmed, E. del Rio-Chanona, and M. Mercangöz, "Comparative study of machine learning and system identification for process systems engineering dynamics," *Industrial & Engineering Chemistry Research*, vol. 64, 02 2025.

[4] S. L. Brunton and J. N. Kutz, *Data-Driven Science and Engineering: Machine Learning, Dynamical Systems, and Control*, 2nd ed. Cambridge University Press, 2022.

[5] A. Simpkins, *System Identification: Theory for the User, 2nd Edition (Ljung, L.; 1999) [On the Shelf]*, 2012, vol. 19, no. 2.

[6] S. Helman, H. Jung, N. Baeckeland, D. Ramasubramanian, and S. Dhople, "Grey-box system identification of grid-forming inverters," in *2024 9th IEEE Workshop on the Electronic Grid (eGRID)*, 2024, pp. 1–6.

[7] M. Al-Greer, M. Armstrong, M. Ahmeid, and D. Giaouris, "Advances on system identification techniques for dc–dc switch mode power converter applications," vol. 34, no. 7, 2019, pp. 6973–6990.

[8] S. Billings, *Nonlinear System Identification: NARMAX Methods in the Time, Frequency, and Spatio-Temporal Domains*, 08 2013.

[9] H. Liu, L. Zhu, Z. Pan, F. Bai, Y. Liu, Y. Liu, M. Patel, E. Farantatos, and N. Bhatt, "Armax-based transfer function model identification using wide-area measurement for adaptive and coordinated damping control," *IEEE Transactions on Smart Grid*, vol. 8, no. 3, pp. 1105–1115, 2015.

[10] M. Korda and I. Mezić, "Linear predictors for nonlinear dynamical systems: Koopman operator meets model predictive control," *Automatica*, vol. 93, pp. 149–160, 2018.

[11] M. Korda, Y. Susuki, and I. Mezić, "Power grid transient stabilization using koopman model predictive control," vol. 51, no. 28. Elsevier, 2018, pp. 297–302.

[12] X. Gong and X. Wang, "A novel koopman-inspired method for the secondary control of microgrids with grid-forming and grid-following sources," *Applied Energy*, vol. 333, p. 120631, 2023. [Online]. Available: https://www.sciencedirect.com/science/article/pii/S0306261922018888

[13] S. Hanke, S. Peitz, O. Wallscheid, S. Klus, J. Böcker, and M. Dellnitz, "Koopman operator based finite-set model predictive control for electrical drives," 04 2018.

[14] O. Azencot, N. B. Erichson, V. Lin, and M. Mahoney, "Forecasting sequential data using consistent koopman autoencoders," in *International Conference on Machine Learning*. PMLR, 2020, pp. 475–485.

[15] S. Golestan, M. Monfared, and F. D. Freijedo, "Design-oriented study of advanced synchronous reference frame phase-locked loops," *IEEE Transactions on Power Electronics*, vol. 28, no. 2, pp. 765–778, 2013.

[16] L. Fan, Z. Miao, S. Shah, Y. Cheng, J. Rose, S.-H. Huang, B. Pal, X. Xie, N. Modi, S. Wang, and S. Zhu, "Real-world 20-hz ibr subsynchronous oscillations: Signatures and mechanism analysis," *IEEE Transactions on Energy Conversion*, vol. 37, no. 4, pp. 2863–2873, 2022.

[17] Y. Cheng, L. Fan, J. Rose, S.-H. Huang, J. Schmall, X. Wang, X. Xie, J. Shair, J. R. Ramamurthy, N. Modi, C. Li, C. Wang, S. Shah, B. Pal, Z. Miao, A. Isaacs, J. Mahseredjian, and J. Zhou, "Real-world subsynchronous oscillation events in power grids with high penetrations of inverter-based resources," *IEEE Transactions on Power Systems*, vol. 38, no. 1, pp. 316–330, 2023.

[18] M. Cespedes and J. Sun, "Impedance modeling and analysis of grid-connected voltage-source converters," *IEEE Transactions on Power Electronics*, vol. 29, no. 3, pp. 1254–1261, 2014.

[19] P. Kundur *et al.*, "Power system stability," *Power system stability and control*, vol. 10, no. 1, pp. 7–1, 2007.

[20] M. Ester, H.-P. Kriegel, J. Sander, X. Xu *et al.*, "A density-based algorithm for discovering clusters in large spatial databases with noise," in *kdd*, vol. 96, no. 34, 1996, pp. 226–231.

[21] X. Luo, Y. Pavan Kumar, A. K. Singh, E. I. Batzelis, G. Saridaki, P. Kotsampopoulos, and N. Hatziargyriou, "Boundary analysis of damping methods for virtual synchronous generators," 2025.

[22] N. R. Guideline, "Bps-connected inverter-based resource performance," Tech. Rep., 2018.

[23] N. Hatziargyriou, J. Milanovic, C. Rahmann, V. Ajjarapu, C. Canizares, I. Erlich, D. Hill, I. Hiskens, I. Kamwa, B. Pal *et al.*, "Definition and classification of power system stability–revisited & extended," *IEEE Transactions on Power Systems*, vol. 36, no. 4, pp. 3271–3281, 2020.

[24] A. J. Wood, B. F. Wollenberg, and G. B. Sheblé, *Power generation, operation, and control*. John wiley & sons, 2013.

[25] M. Klein, G. J. Rogers, and P. Kundur, "A fundamental study of inter-area oscillations in power systems," *IEEE Transactions on power systems*, vol. 6, no. 3, pp. 914–921, 1991.